Supplementary

1.

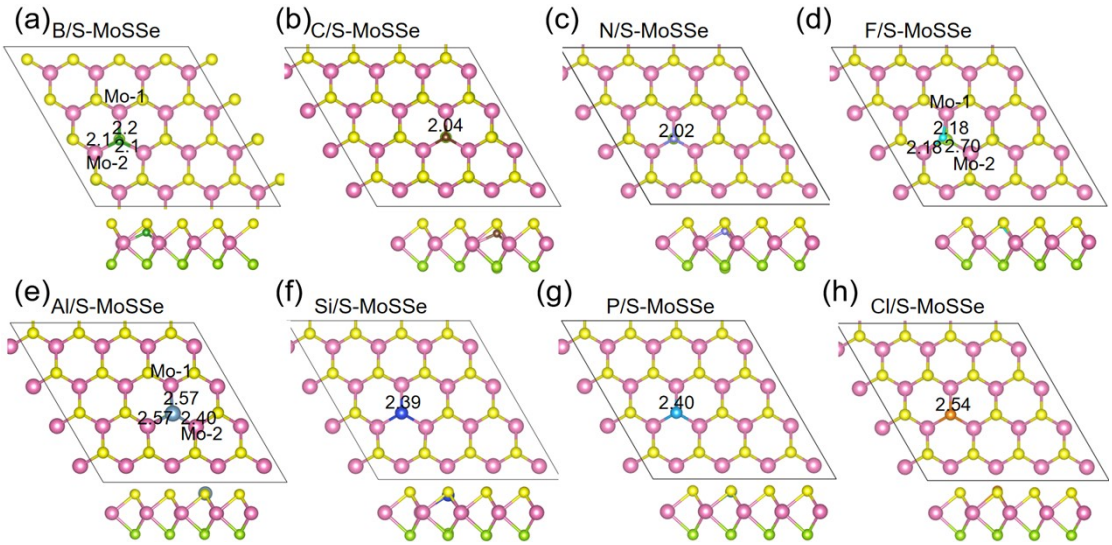

SFig.1 The top and side views of (a) B/S-MoSSe, (b)C/S-MoSSe, (c) N/S-MoSSe, (d) F/S-MoSSe, (e) Al/S-MoSSe, (f) Si/S-MoSSe, (g) P/S-MoSSe, (h) Cl/S-MoSSe. Pink, green and yellow balls are respectively Mo, Se and S atoms. The 4×4 supercell of the MoSSe Janus monolayer is represented by the black rhombus.

STable.1 The formation energies (E_f), the bond lengths of X-Mo, the energy difference (ΔE) between the ferromagnetic state and paramagnetic state of MoSSe (X represents B, Al, C, Si, N, P, F and Cl atoms respectively) substitutional doping both with S and Se sites.

		X-M(Å)	E_f(eV)	Chg(eV)		M(μ_B)	
				S(Se)	Mo	S(Se)	Mo
B	Se	2.11	-6.64	3.23	5.08	0.09	0.17
	S	2.10/2.20	-5.18	3.28	5.12	0.13	0.06/0.33
Al	Se	2.52	-6.58	1.86	5.43	0.0	0.24
	S	2.49/2.57	-5.19	1.87	5.42/5.56	0.0	0/0.37
C	Se	2.02	-6.69	4.76	4.94	0.0	0.0
	S	2.04	-5.24	4.76	4.97	0.0	0.0
Si	Se	2.37	-6.63	3.62	5.23	0.0	0.0
	S	2.39	-5.16	3.69	5.27	0.0	0.0
N	Se	2.01	-6.71	5.97	5.05	0.24	0.0
	S	2.02	-5.26	5.95	4.90	0.24	0.0
P	Se	2.42	-6.65	5.42	5.06	0.10	0.0
	S	2.40	-5.13	5.34	5.12	0.33	0.0
F	Se	2.28	-6.64	7.69	4.97	0.10	0.21
	S	2.18/2.70	-5.17	7.66	5.09/4.97	0.0	0.0/0.65
Cl	Se	2.54	-6.59	7.50	5.03	0.0	0.25
	S	2.54	-5.14	7.46	5.09	0.0	0.25

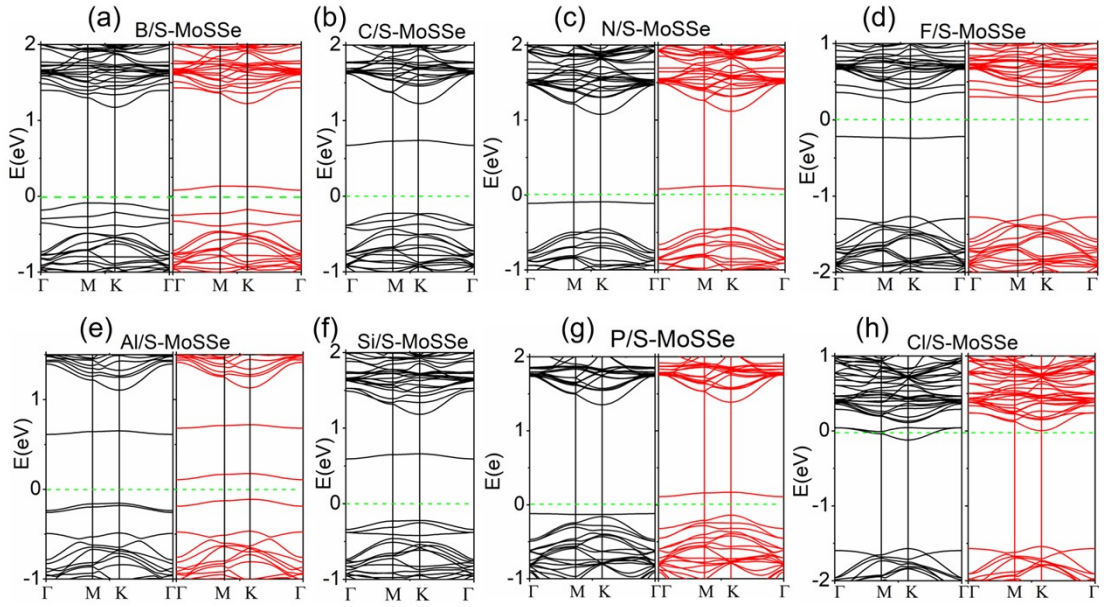

SFig.2 The electronic bands of (a) B/S-MoSSe; (b) C/S-MoSSe; (c) N/S-MoSSe; (d) F/S-MoSSe; (e) Al/S-MoSSe; (f) Si/S-MoSSe; (g) P/S-MoSSe; (h) Cl/S-MoSSe. The Fermi level has been set to zero, which has been denoted as the green dashed lines.

We have compared the effects of substituting selenium (Cl/Se-MoSSe) and sulfur (Cl/S-MoSSe) atoms respectively in a (4×4) supercell of the MoSSe monolayer with chlorine atom. Our calculation point out that the structural and electronic effects of substitutional doping in Janus MoSSe monolayers exhibit a pronounced site-dependence, particularly when comparing S-site versus Se-site doping. This asymmetry originates from the intrinsic structural polarity of the MoSSe monolayer, where the S–Mo bond (~2.42Å) is notably shorter and stronger than the Se–Mo bond (~2.53 Å). Consequently, substituting the smaller, more electronegative S atom, especially with dopants whose atomic radii and electronegativities differ significantly from S, such as B, Al, and F, induces more substantial local lattice distortion compared to Se-site doping. Key structural differences are summarized in Supplementary STable.1. It is found that there are two major observations emerging from the S-site doping analysis. At the doping site of B, Al and F doped MoSSe monolayer, the local threefold rotational symmetry is broken, and instead of three equivalent X–Mo bonds, two bonds become slightly shorter while the third elongates by approximately 0.5 Å. This significant structural distortion directly perturbs the local electronic environment. Therefore, the elongated X–Mo bond leads to incomplete passivation of the electronic states on the adjacent Mo atom, resulting in the formation of localized impurity states near the Fermi level. Under spin-polarized conditions, these states become spin-split and stabilize in ferromagnetic configuration. Therefore, in contrast to the Se-site doped MoSSe monolayer, B-, Al-, and F-doped MoSSe at the S-site consistently exhibit ferromagnetic ordering.

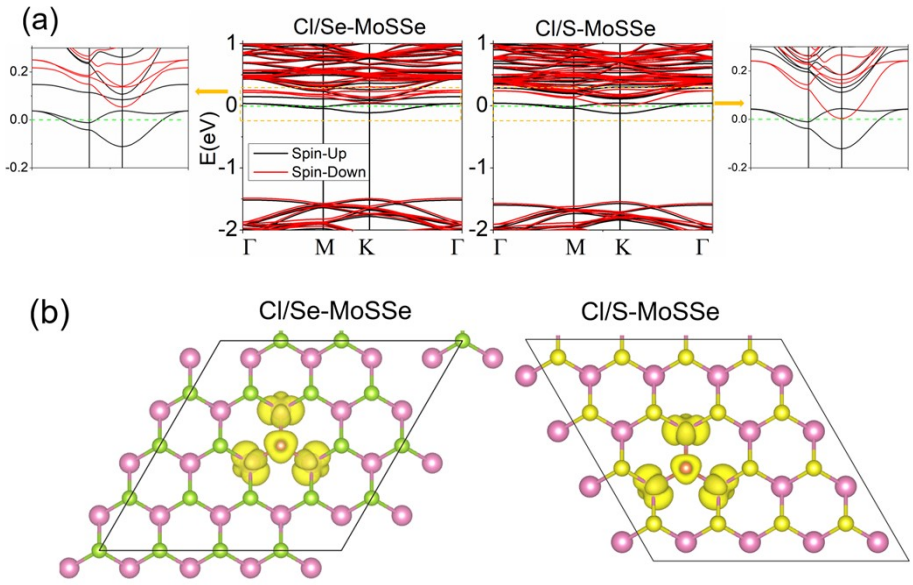

SFig.3 (a) The spin-polarized of Cl/Se-MoSSe and Cl/S-MoSSe. Here, the Fermi level has been set to zero and is labeled by green dashed lines. The left and right panels are enlarged sections within the orange dashed boxes. (b) The spin-polarized charge density of Cl/Se-MoSSe and Cl/S-MoSSe. The yellow isosurfaces represents spin-up states and the isovalue is 0.01 e/bohr^3. The pink, green, yellow and orange balls respectively denote Mo, Se, S and Cl atoms.

While it is important to pointed that the C, Si, N, P and Cl doped MoSSe monolayer both at S and Se sites exhibit nearly identical electronic and magnetic properties. Taken Cl/S-MoSSe, as shown in SFig. 2(h), both systems display spin polarization near the Fermi level, exhibiting ferromagnetic stability and half-metallic behavior. Specifically, the spin-down channel is semiconducting with direct band gaps of 1.55 eV for Cl/Se-MoSSe and 1.54 eV for Cl/S-MoSSe, while the spin-up channel remains metallic. A notable difference, however, is that the conduction band minimum of the spin-down channel in Cl/S-MoSSe lies only 0.0036 eV below the Fermi level, making it more susceptible to external perturbations—such as substrate-induced strain—that could drive a phase transition. The spin charge density distribution, presented in SFig.S1(b), indicates that the spin-polarized electrons are primarily localized around the doped Cl atom and its bonded Mo atom in both configurations.

In summary, the site-specific structural response to doping, driven by the inherent bond strength difference between S–Mo and Se–Mo, plays a decisive role in determining the resulting electronic and magnetic properties.

2. Here, we present the energy evolution as a function of simulation steps, along with the final structural diagrams, for both single-atom (SFig.4) and dual-Cl (SFig.5) doped MoSSe systems obtained from molecular dynamics simulations at room temperature(300K). The simulations were carried out for 5000 steps in total, and the plots depict the energy variation during the last 1000 steps, which correspond to the thermodynamic equilibrium stage. As shown in the SFig.4 and SFig.5, once equilibrium is reached, the energy of each system fluctuates only slightly with simulation time, and the atomic structures remain intact. These results indicate that MoSSe doped with non-magnetic atoms exhibits excellent structural stability at room temperature, suggesting its potential for experimental synthesis.

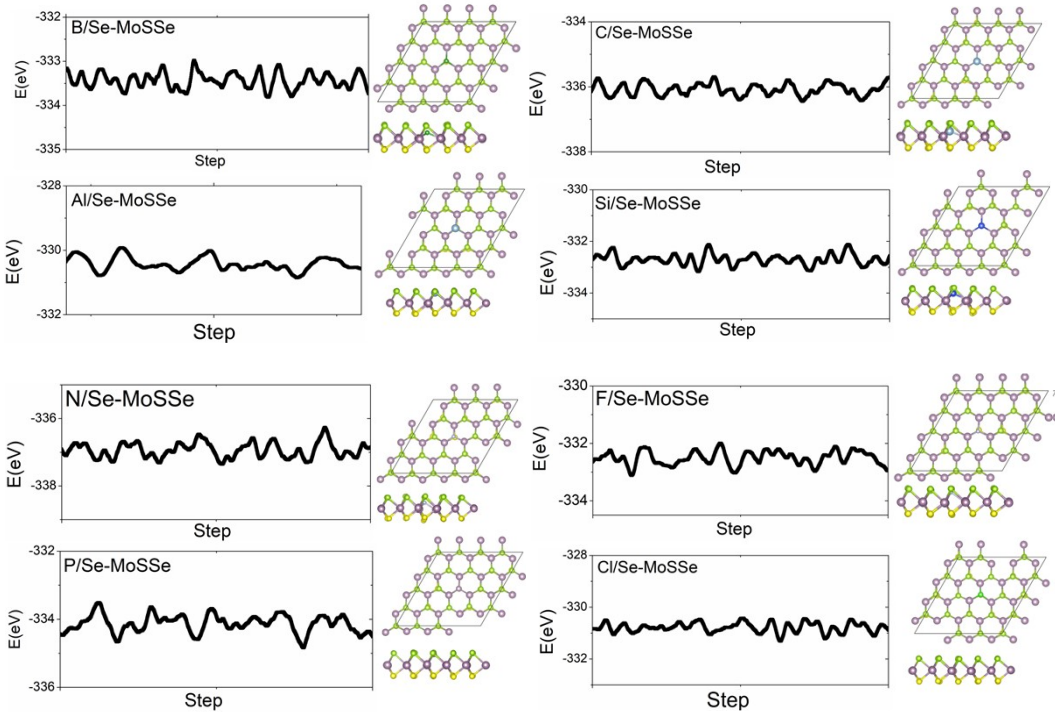

SFig.4 The energy of single-atom doped MoSSe monolayer varies with simulation steps during the last 1000 steps and each corresponding atomic structures at last step.

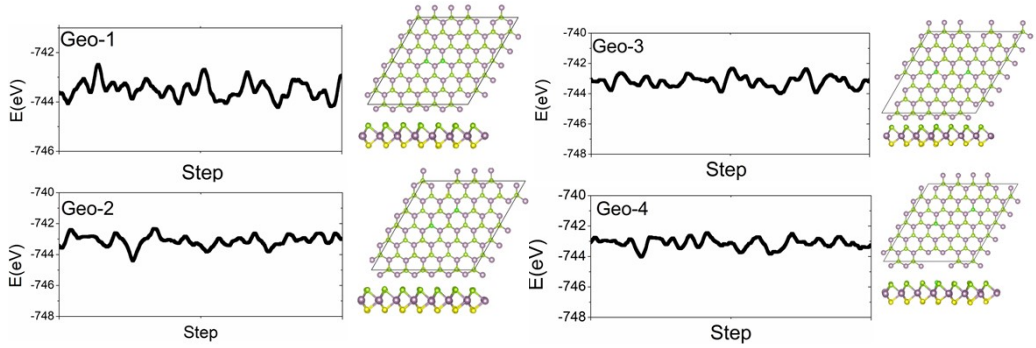

SFig.5 The energy of dual-Cl doped MoSSe monolayer varies with simulation steps and its atomic structures at last step.

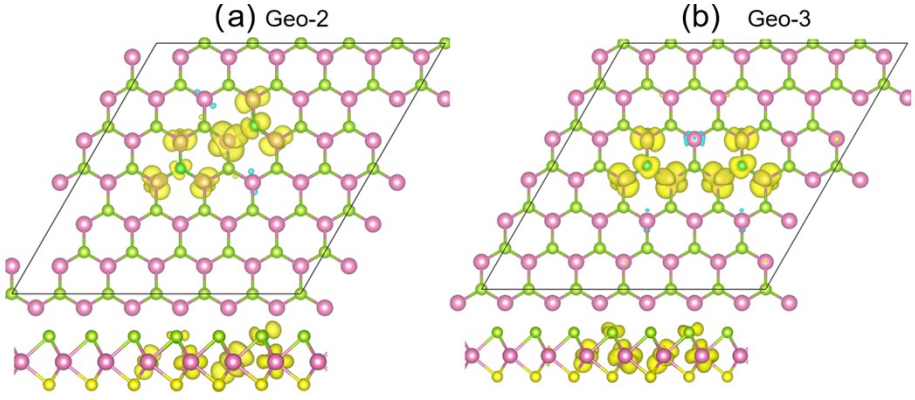

3.

SFig.6 The spin charge densities of (a) Geo-2 and (b) Geo-3. The yellow isosurfaces represents spin-up states and the isovalue is 0.01 e/bohr^3. The purple and green balls respectively denote the Ge and Se atoms.

Similarly, in Geo-2, the distance between Mo-4 and Cl-2 is 2.81 Å, which is much larger than the Mo-Cl bond length of 2.50Å, while the other Mo–Cl bond lengths range from 2.50 to 2.55 Å. Consequently, the Mo-4 here remains incompletely passivated, leading to a relatively localized electronic distribution near the Fermi level and a correspondingly larger magnetic moment of 0.58 μB. Based on our ferromagnetic state calculations, the magnetic moments on the other Mo atoms are relatively small, respectively 0.15 μB on Mo-1, 0.23 μB on Mo-2, and 0.14 μB on Mo-2, as shown in SFig.6(b). In contrast, the Cl–Mo bond lengths in Geo-3 range from 2.50 to 2.58 Å, indicating minimal structural perturbation in it. During ferromagnetic state calculations, similar to the single Cl-doping case, small magnetic moments are distributed on the Mo atoms near the doping centers in Geo-3, as shown in SFig. 6(b). Specifically, the moments are 0.16 μB on Mo-1, 0.20 μB on Mo-2, and 0.29 μB on Mo-3. However, due to the close proximity of the magnetic centers in both Geo-2 and Geo-3, the magnetic interactions between them are strong. Our total energy calculations reveal that the paramagnetic (PM) state is more stable than the ferromagnetic (FM) state in these configurations, with the PM state being lower in energy by 15 meV for Geo-2 and 23 meV for Geo-3. Therefore, the paramagnetic state is the ground state for both Geo-2 and Geo-3.